



Investigation into the influence of boronizing on the wear behavior of additively manufactured Inconel 625 alloy at elevated temperature

A. Günen¹ · U. Gürol^{2,3} · M. Koçak⁴ · G. Çam⁵

Received: 13 August 2022 / Accepted: 7 January 2023
© The Author(s), under exclusive licence to Springer Nature Switzerland AG 2023

Abstract

Directed energy deposition (DED) technology is a cost-effective additive manufacturing method widely used in the production of complex-shaped parts made of various engineering alloys as well as superalloys due to its advantages such as high deposition efficiency, low-cost and flexible production possibilities. However, in addition to the low surface hardness found in wrought superalloys, the very high heat input and severe elemental segregation during the manufacture of superalloys by DED often result in diminishing of wear performance further. In this study, a simultaneous heat treatment and boronizing (980 °C 1 h) was applied to Inconel 625 part produced by the GMAW-based DED process in a single process in order to improve its microstructure and its tribological properties. The effects of boronizing applied after the DED process on the microstructure, some mechanical properties and wear behavior (both at room temperature and 500 °C) were investigated.

Keywords Directed energy deposition · Additive manufacturing · Superalloy · Gas metal arc welding · Boronizing · High-temperature wear

1 Introduction

Additive manufacturing (AM) is an innovative production process that enables the desired machine parts to be produced more cost-effectively than traditional production processes, using a layer-by-layer deposition mechanism by combining volume elements called voxels (the 3D equivalent of a pixel). Ikeo et al. defined additive manufacturing as the conversion of a triangular lattice model, which is another

type of 3D CAD model, into a part layer by layer with the help of a three-dimensional printer after decomposing it into layers with special software [1]. Smith et al. reported that many materials can be produced by AM method, including polymeric materials, biological materials and metallic materials [2]. In addition, fabrication of metallic components by AM has become one of the most important research topics in materials science and mechanical engineering in the last decade.

Kannan and Rajendran suggested that AM's ability to realize the concept of "near net shape production" makes this method one step ahead of machining processes in the production of complex geometries [3]. It is also worth noting that AM's other advantages include tailor-made production, sustainable production and energy efficiency. It has been reported by many researchers [2, 4–8] that these advantages enable the AM method to be used increasingly more widely in several industries such as automotive, aviation, space, health, construction and energy.

Özer reported in a review study on additive manufacturing technologies that, although the idea of additive manufacturing dates back to very old times, the first emerging system started with the plastic processing technique known as the SL (stereolithography) technique in 1987, and this development was followed by the introduction of additive

✉ G. Çam
gurel.cam@iste.edu.tr

¹ Faculty of Engineering and Natural Sciences, Department of Metallurgy and Materials Engineering, Iskenderun Technical University, 31200 Iskenderun-Hatay, Turkey

² Faculty of Engineering, Department of Metallurgical and Materials Engineering, Istanbul Gedik University, Istanbul, Turkey

³ Gedik Welding Company, Research and Development Center, Istanbul, Turkey

⁴ Faculty of Engineering, Department of Mechanical Engineering, Istanbul Gedik University, Istanbul, Turkey

⁵ Faculty of Engineering and Natural Sciences, Department of Mechanical Engineering, Iskenderun Technical University, 31200 Iskenderun-Hatay, Turkey

manufacturing technologies such as Fused Deposition Modeling (FDM), Solid Ground Curing (SGC) and Laminated Object Manufacturing (LOM) to the market in the 1990s [9]. He also stated that the Selective Laser Sintering (SLS) method, which is the cornerstone for the most important developments for the metal industry, was developed shortly after these methods.

In the past 20 years, developments in additive manufacturing technologies have accelerated considerably particularly with the progress in use of metallic powder and solid wire as consumables together with the robotics. As existing technologies continue to evolve, important new technologies such as Direct Metal Laser Melting (DMLM) have been developed and commercialized. In 2002, sales of Direct Metal Deposition (DMD) systems were started. At the beginning of 2016, a new technology, a new product, a new material or a new application appeared almost every week and AM processes began to be classified based on many parameters. These systems have become more reliable and more efficient as time has passed, and the variety of suitable materials for these production methods has increased significantly [10–12].

Because metals can preserve their superior mechanical properties at elevated temperatures, metal additive manufacturing, which is basically based on the well-known welding processes, has found wide-range applications in production of advanced engineering components. Fang et al. defines metal additive manufacturing (MAM) as a technology that can be used to build parts to be produced layer by layer, allowing the manufacture of parts with more complex geometry and at lower costs compared to traditional manufacturing techniques [13].

The American Society for Testing and Materials (ASTM) has classified MAM techniques for metallic materials as (a) powder bed fusion, (b) directed energy deposition, and (c) sheet lamination. Tofail et al. reported that among these methods, powder-based MAM methods (for example, selective laser melting (SLM) and electron beam melting (EBM)) are widely used [14]. However, Gebhardt and Hötter stated that a laser or electron beam is used to selectively melt and sinter the particles in powder-based systems, and difficult system control procedures, post-treatment requirements, high residual stress, undesirable porosity formation, high heat input and finally problems associated with system setups and powder costs make this process difficult to implement in small and medium-sized enterprises (SMEs) [15]. In contrast, many other researchers [16–18] have reported that arc-directed energy deposition systems (wire fed arc welding systems) are more common in the market due to its advantages, such as being less complex than powder bed fusion systems, lower initial setup cost, higher deposition rate, and better energy efficiency than powder-based laser/electron beam assisted deposition methods or laser/

electron-directed energy deposition systems. With these advantages, arc-directed energy deposition processes have become an attractive manufacturing process to MAM researchers and manufacturers, especially SMEs interested in using manufacturing processes with innovation.

Arc-directed energy deposition (Arc-DED) systems, also known as wire arc additive manufacturing (WAAM), is a technology that has an important share among advanced manufacturing technologies, particularly for complex-shaped medium-to-large sized metallic parts. Unlike other additive manufacturing (AM) technologies, Arc-DED uses an electric arc as a heat source to deposit the metallic material layer by layer (as a well-known welding process) that makes up the fabricated product. According to the type of heat source employed, there are 3 Arc-DED methods, namely Gas Tungsten Arc Welding (GTAW) based, Gas Metal Arc Welding (GMAW) based and Plasma Arc Welding (PAW) based Arc-DED [18, 19]. Xia et al. also reports that the Arc-DED method stands out as it has higher deposition rates and requires lower cost equipment than wire laser or electron additive manufacturing methods, and offers more environmentally friendly production processes compared to powder-fed additive manufacturing processes [19]. In addition, Nagasai et al. also claimed that the Arc-DED (WAAM) process has become a viable advanced manufacturing technique in the production of large-scale parts with complex geometry due to its high deposition rate and low-cost advantages [20]. Production of Inconel with the WAAM method has advantages such as high deposition efficiency, low-cost and flexible production possibilities compared to production by casting and forging method. In addition, production with the WAAM method does not require molds, which cause great costs in conventional manufacturing methods such as forging and casting [17, 21]. However, there are some process-related difficulties that prevent the widespread integration of Arc-DED into various manufacturing industries. Harris listed these problems as lack of process robustness, stability and repeatability [21]. In this context, this study aimed to provide further insight into the surface functionalization of the Arc-DED-produced Inconel 625 alloy.

Nickel-based superalloys, which are used in advanced engineering applications, such as turbine blades and combustion chambers, due to their excellent tensile strength, high-temperature yield strength, creep properties and corrosion resistance [22–24], are among the most preferred additive manufacturing applications [13]. The manufacturing processes of these AM products are extremely important because the mechanical properties of these alloys depend not only on grain size and microstructural texture, but also on the precipitate distribution of the layer-by-layer deposited material. For example, the occurrence of Nb segregations in the interdendritic regions during solidification results in the formation of Laves phases, which increases the brittleness

of the alloy. To overcome these problems, it is suggested that a homogenization heat treatment is usually applied after the AM process, which improves the microstructure and mechanical properties [25, 26].

Another study applying secondary heat treatment to Inconel 625 alloy is conducted by Safarzade et al. [27]. In their study, the authors applied homogenization at 1100 °C for 6 h, followed by cooling in water, homogenization at 1100 °C for 6 h, and then aging at 700 °C for 24 h followed by cooling in water. They reported that the microstructure of the as-prepared Arc-DED samples consisted of a dendritic Ni-based solid solution phase containing (Nb,Ti)C carbide, Laves and δ -Ni₃Nb secondary phases. They reported that after the applied heat treatment, Laves and Ni₃Nb phases dissolved and the dendritic grains turned into large columnar grains. They also reported that the aging process after the heat treatment led to the formation of grain boundary M₂₃C₆ carbide and nanometric γ' precipitates. The authors observed that the hardness, yield and tensile strengths and % elongation values of the samples prepared by the Arc-DED method were close to the cast Inconel alloys, and the homogenization heat treatment improved the hardness and yield strength, but decreased the % elongation but did not have a significant effect on the tensile strength. They further reported that in contrast to homogenization aging heat treatment causes deterioration of tensile properties and transforms the fracture mode into a mixture of intergranular ductile and intergranular brittle one, thus negatively affecting mechanical properties.

On the other hand, many researchers indicated that it is of great importance to cover the surfaces of Ni-based superalloys with a hard layer when used in abrasive environments due to their low hardness despite their mechanical stability at high temperatures and their resistance to oxidation and corrosion [28–31].

Boronizing processes are one of the most frequently applied methods to improve the wear resistance of Ni-based superalloys. There are many studies reporting that the wear resistance of Ni-based superalloys is improved both at room temperature and elevated temperatures by obtaining complex boride layers containing NiB, CrB, FeB, and NbB with surface hardness in the range of 2000–3500 HV due to the affinity of the alloying elements existing in the alloy, namely Ni, Cr, Fe, Nb, etc., against boron. For example, Campos-Silva et al. conducted 50, 100, 150 and 200 dry shear wear tests on different boride coating thicknesses which they obtained after boronizing the Inconel 718 alloy for 2 h at 900 °C and 6 h at 950 °C [31]. In their study, the authors reported that the presence of a deeper compressive residual stress zone that occurs in samples boronized at 950 °C for 6 h increases the wear resistance approximately two to three times compared to samples boronized at 900 °C for 2 h. In another study,

Güven reported that the boride layers formed on the surface of the Inconel 718 super alloy maintain their existence up to 750 °C, and thus improve the high-temperature wear resistance of these alloys [32]. In addition, Makuch et al. reported that the nickel–chromium boride layers formed on the surface of Nimonic 80A alloy have a hardness value in the range of 1160–2132 HV, the cohesion between the produced boride layers and the substrate material is in HF3 quality, and as a result, an improvement in wear resistance exceeding six times is achieved [33]. Therefore, it is thought that a similar improvement can be obtained in the samples produced by the Arc-DED method by boronizing heat treatment which is well demonstrated to improve the wear resistance of wrought superalloys.

For this purpose, boronizing treatment for 1 h at 980 °C was applied to Inconel 625 alloys produced by the Arc-DED (WAAM) method in this study, which is determined to be the best heat treatment from the literature providing the optimum results in the microstructure and mechanical properties of these alloys. Thus, the samples produced with Arc-DED were both heat treated and their surfaces hardened simultaneously. Then, the microstructure, hardness, modulus of elasticity, wear behavior at room temperature and at 500 °C of Inconel 625 alloys samples in wrought, Arc-DED-fabricated and Arc-DED-fabricated + borided conditions were investigated. The results show: (i) The heat treatment applied after the deposition process refined the grain size of the dendrites; (ii) The heat applied during boronizing minimized the segregation by promoting the diffusion of elements such as Nb and Mo in the interdendritic structures; (iii) Boronizing has increased the hardness value of Inconel 625 alloy produced by the Arc-DED process up to 10 times; and (iv) The increase in surface hardness and modulus of elasticity resulted in an improvement in wear resistance exceeding 58.17 times at room temperature and up to 3.86 times at 500 °C wear conditions. The temperature of wear test has a great influence on the coefficient of friction and wear rates. Namely, the wear mechanism of both wrought Inconel 625 alloy and non-boronized Inconel 625 alloy fabricated by the Arc-DED process at room temperature was abrasive and severe plastic deformation, while the wear mechanism at 500 °C turned into oxidative supported adhesion wear. On the other hand, the wear mechanism of the boronized Inconel 625 alloy fabricated by the Arc-DED process at room temperature was micro-crack and oxidative wear mechanism, and it turned into an oxidation-assisted polishing wear mechanism at 500 °C. In the study, it was also determined that boronizing as a secondary process applied to the additive manufactured parts by the Arc-DED method refines dendrite grain size, minimizes segregation and significantly improves the wear resistance of Inconel 625 alloy.

Table 1 Typical chemical composition and standard ranges (wt. %) of the filler metal used as well as the average of the 9 analyses conducted in three locations (lower, middle and upper part, 3 analyses at each location) of the deposited Inconel 625 wall structure

Standard	Ni	Cr	Mo	Nb	Fe	Ti	Al	Si
AWS A5.14	min. 58	20–23	8–10	3.15–4.15	max. 5.0	max. 0.4	max. 0.4	max. 0.5
	Cu	Mn	C	P	S	–	–	–
	max. 0.5	max. 0.5	max. 0.1	max. 0.02	max. 0.015	–	–	–
ERNiCrMo3	Ni	Cr	Mo	Nb	Fe	Ti	Al	Si
	64.85	21.15	8.67	3.54	1.15	0.22	0.13	0.06
	Cu	Mn	C	P	S	–	–	–
Deposited Inconel 625 wall structure	Ni	Cr	Mo	Nb*	Fe**	Ti	Al	Si
	65.08	20.48	9.12	4.25	0.54	0.2	0.12	0.06
	Cu	Mn	C	P	S	–	–	–
	0.23	0.0	–	0.051	0.073			

* Nb content was higher than the maximum limit (of the standard) in all the analyses conducted, and ** Fe content higher than the maximum limit only in three analyses conducted at the bottom part of the wall structure

Table 2 Typical mechanical properties of the filler metal used

	Yield strength (MPa)	Ultimate tensile strength (MPa)	Elongation (%)	Charpy Impact Toughness (J at 20 °C)
ERNiCrMo3	540	800	38	140

2 Experimental procedure

2.1 Arc-DED process

The single-walled Arc-DED process was carried out on a S304 stainless steel substrate of 12 mm thick, 75 mm wide and 350 mm long. The solid wire of ER NiCrMo 3 (acc. to AWS A5.14) having 1.2 mm diameter was used as filler metal. The typical chemical analysis of the wire used obtained by XRF analysis is given in Table 1 together with the typical chemical composition of it according to AWS A5.14 standard, while Table 2 shows the mechanical properties obtained by the wire used.

The GeKa-Tec WB 500L welding (Gas Metal Arc Welding—GMAW) machine with a water-cooled torch integrated on a 6-axis OTC Daihen D-V8L industrial welding robot was operated as the power source of Arc-DED system (Fig. 1). The substrate surface was cleaned to remove the grease or oil with acetone before the deposition process. The deposition directions of two consecutive layers were reverse, and the first layer was deposited in the clockwise direction. It is known that the inter-layer cooling time directly influences the temperature distribution of the thin-walled components produced by Arc-DED [34], and therefore, after the deposition of each layer, the torch was lifted by 1.6 mm and a waiting time of 120 s is

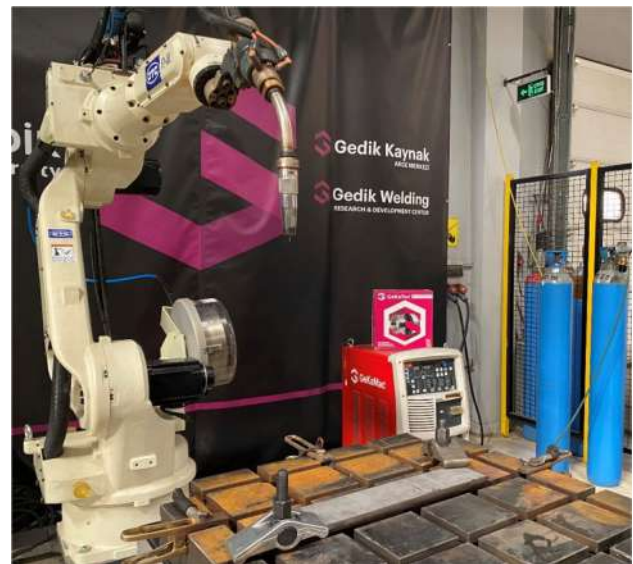


Fig. 1 The robotic Arc-DED setup used to produce Inconel 625 wall

employed to help the component transfer excessive heat to the environment (for each layer for sufficient refining of the previously deposited layer). 97.5% Ar + 2.5% CO₂ was used as the shielding gas with the flow rate of 15 L/min. The contact tube-to-work piece distance was 12 mm.

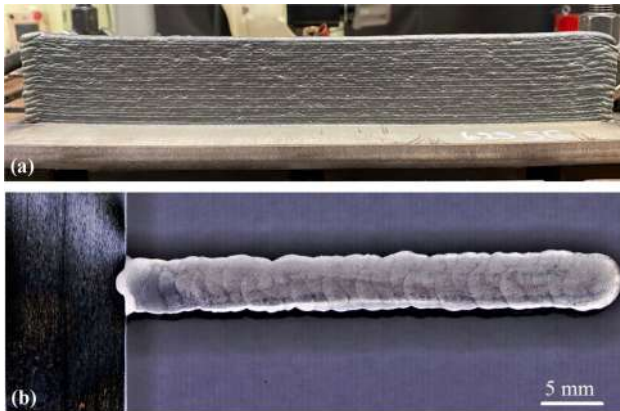
The temperature after each 5th layers before deposition of the next layer were measured using the infrared thermometer and results are shown in Table 3. The main processing parameters involved in the deposition process are given in Table 4. The blade-like wall component was fabricated by depositing total of 30 layers, each layer being about 300 mm in length, 50 mm height and 6.5 mm in thickness (Fig. 2). The chemical composition of the wall component (which is the average of nine XRF analyses conducted at three

Table 3 The temperature variation between the each 5th layers

Filler wire	5th layer	10th layer	15th layer	20th layer	25th layer	30th layer
625 SG	95 °C	135 °C	165 °C	171 °C	192 °C	212 °C

Table 4 Process parameters use in the Arc-DED process

		SG625
Current	A	150
Voltage	V	15.8
Travel speed	cm/min	50
Shielding gas		Ar 97.5% + CO ₂ 2.5%
Gas flow rate	l × min ⁻¹	15
Contact tube to work piece	mm	12
Torch angle	°	Neutral (°)
Arc length	mm	10
Dwell time	seconds	120

**Fig. 2** Additively manufactured Ni-based superalloy Inconel 625 wall component: **a** general view and **b** optical macrograph showing the cross-section

different locations, namely bottom, middle and top section, three analyses at each location) is given in Table 1. To detect any defects which may be present in the manufactured component, X-ray radiographic test (RT) was conducted according to EN ISO 17636–1. The macroscopic evaluation was carried out in accordance EN ISO 17639 to detect any solidification cracks or insufficient melting between the layers. In addition, extensive microhardness measurements were conducted across the wall structure fabricated by Arc-DED along the building direction using a load of 5 kg in order to determine the hardness distribution.

The X-ray test results revealed that the deposited wall structure was free of porosity, insufficient melting and solidification cracks and met the minimum requirements of the ISO 5817 Class B standard. Moreover, the microscopic

observations conducted on different regions proved this. The deposited wall structure seems to have a uniform surface finish from the visual appearance after the whole manufacturing process. These results indicate that the applied WAAM parameters yield the defect-free Inconel 625 wall structure in the current work.

2.2 Boronizing process

Prior to the boronizing, the samples (25 × 20 × 5 mm) extracted from the component fabricated by Arc-DED were ground and polished up to 800 grid SiC abrasive paper. Bagherzadeh et al. reported that although additive manufacturing technologies offer the manufacture of highly complex parts, the parts produced generally have poor surface quality and must be machined with a secondary machining method [35]. Therefore, approximately 40 μm of ESD coating layer was removed from the surface of the samples to achieve optimum surface roughness. As can be seen in Fig. 2, the samples produced with Arc-DED displayed a surface with a higher surface roughness compared with the machined surfaces. However, the wall structure fabricated in the current study exhibits a surface roughness, Ra, of 74,2 μm in the as-deposited condition, which is considered to be significantly better compared to the existing literature [36–38]. Thus, the wall structure fabricated is considered to be a high-quality part. Then, the surfaces of the specimens extracted from the wall structure were subjected to milling machining up to < 1 Ra value on the CNC machine followed by grinding with SiC sand papers with the grids between 320 and 1000 until an optimum surface roughness of < 0.25 Ra is achieved, prior to boriding.

Based on previous studies in the literature [31, 32, 39], B₄C and NaBF₄ powders were selected for the boronizing process in order to prevent unwanted silicide formation in Ni-based alloys. Boronizing of Ni-based superalloys can be performed in the temperature range of 850–1050 °C and for 1–12 h, as the case in steels as pointed out by various researchers [40–42]. Moreover, Tanvir et al. reported that they conducted various heat treatments to improve the mechanical properties of the Inconel 625 alloy component produced by Arc-DED and obtained the best mechanical properties after a heat treatment at 980 °C for 1 h [25, 26]. Thus, it was decided to perform the boronizing process at 980 °C for 1 h in an open-air environment. As a result, the samples extracted from the Inconel 625 alloy component produced by Arc-DED were heat treated and boronized simultaneously in a single process.

2.3 Characterization and high-temperature wear testing

Boronized and non-boronized samples were cut with a precision cutting device in the size of $10 \times 10 \times 5$ mm for microstructural analysis. The cross-sectional surfaces of the samples were mounted to be machined. After the conventional grinding and polishing processes were carried out, the mounted samples were finally etched using 1 ml of HNO_3 and 3 ml of HCl with an etching duration of 10 s. SEM and EDS microstructure evaluations of the polished samples were performed using a Circular Backscatter (CBS) detector, with a 20 kV acceleration voltage and a 10 mm spot size using Thermo Fisher Scientific Apreo S LoVac SEM device. XRD analyzes were carried out by examining the surfaces of the samples cut with the size of $20 \times 20 \times 5$ mm from both boronized and non-boronized samples. A Computer-controlled Panalytical Malvern Panalytical Empyrean (Netherlands) XRD instrument was used to determine the XRD patterns. Scanning parameters used in XRD analyzes were determined as: step size 0.0525211, scan angle 2θ angles ranging from 10 to 90° , and $\text{Cu K}\alpha$ radiation (1.5418 \AA). Phase matching was carried out with PDXL software. The surface roughness of the samples before and after boronizing was measured with the Profilm 3D profilometer (Filmetric, USA) device at a speed of 0.1 mm/s and a scan length of 4.8 mm was scanned, and representative 2D profiles were extracted from the 3D images obtained.

Nano-indentation studies were carried out to determine both the hardness and elasticity modulus values of the samples with a single device. They were performed with a Berkovich tipped nano-indentation Hysitron TI-950 TriboIndenter (Germany) with 10 mN load and 30 s constant loading rate, 15 s dwell time and 30 s gradually unloading time. The equations used in the calculations of nano-hardness and modulus of elasticity are given in a previous study carried out by Oliver and Pharr [40]. The nano-hardness and elasticity modulus values were determined by taking the average of at least five different measurements.

Dry sliding ball-on disc wear tests were applied to compare the tribological behavior of the samples extracted from wrought Inconel 625, unboronized and boronized Inconel 625 fabricated by Arc-DED at room temperature and 500°C . Wear tests were carried out using Turkyus POD&HT&WT, (Turkey) ball-on disc device with a high-temperature cell, based on a 10 N load and 250 m sliding distance against a 6.3 mm diameter ball with a hardness of 19 GPa and a modulus of elasticity of 400 GPa. The friction coefficients were recorded automatically based on the transfer of the data received by the load cell on the wear device to the TURKYUS software on the computer. Each wear test was repeated three times to minimize standard deviations. Calculation of the wear volume losses on the worn surfaces after

the wear tests were carried out with a 3D optical profilometer (Profilm 3D, Filmetric, USA) and the worn volumes were calculated automatically. For this purpose, representative 2D profiles were extracted from the obtained 3D images and their corresponding areas were multiplied by the perimeter of the wear traces. Furthermore, the determination of the wear mechanisms on the worn surfaces was carried out by SEM and EDS analysis.

3 Results and discussion

3.1 Microstructure, X-ray diffraction and hardness

Figure 3 reveals the microstructures of the as-Arc-DED manufactured Inconel 625 wall at bottom, middle and the top regions of the building direction. The variation in the microstructure in the difference regions depends on the cooling rate and heat dissipation during the layer depositions as also pointed out by Yangfan et al. [44]. The bottom region is mainly composed of a fine cellular structure due to the substrate's high cooling effect. However, similar microstructures were observed in the middle and top regions having a typical columnar dendritic grain structure with elongated and cellular patterns. The reason for obtaining a similar microstructure throughout the wall structure from the bottom to the top region is the interpass cooling strategy used in the building process, which helped the transferring of the excessive heat to the environment and reduced the heat accumulation of the previously deposited layers and led to a similar solidification rate for each layer. Moreover, the dendrite growth direction was found to be mostly perpendicular to the substrate and the previously deposited layers in all regions.

Figure 4 shows the hardness distribution in the as-Arc-DED manufactured Inconel 625 wall structure along the building direction of 30 layers. As seen from this hardness profile, a relatively homogeneous hardness distribution across the wall structure was obtained as a result of using intervals of 120 s after the deposition of each layer prior to the next layer. There is only a slight hardness decrease at the upper end section of the wall structure due to the accumulation heat. These results are in good agreement with the microstructural observations which revealed a similar microstructure across the deposited wall structure.

The slight decrease in hardness at the upper end section can be explained as follows: Although there is a waiting time between layers for lowering the excessive heat, the interpass temperature increases with increasing number of layers (Table 3). Especially toward the last passes, the interpass temperature rises above 200°C . Thus, as it rises toward the upper layers, both the distance from the substrate and the increase in the temperature of the substrate and the increase of the interpass temperature cause the microstructure to

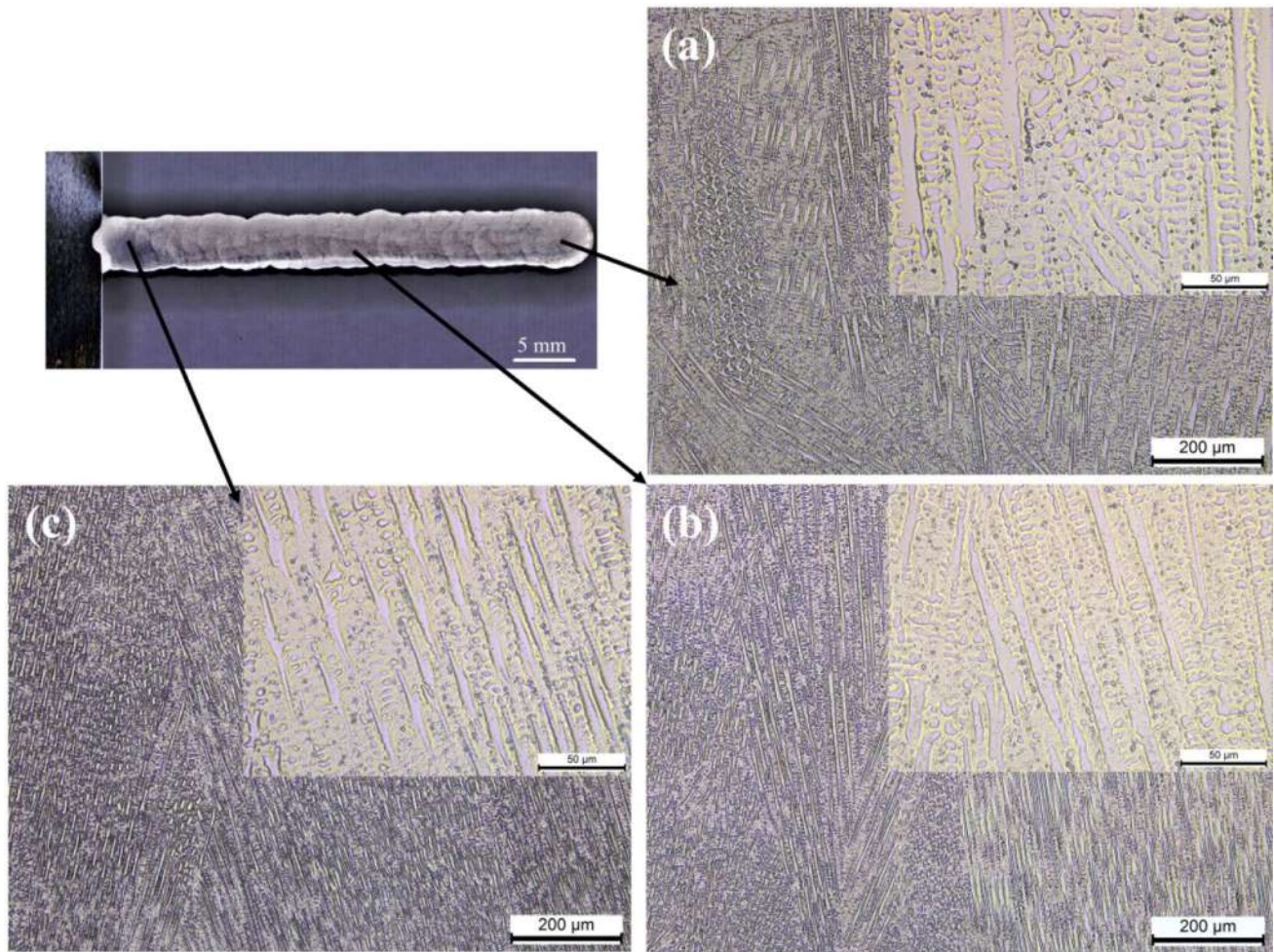


Fig. 3 Microstructures of the as- Arc-DED manufactured Inconel 625 wall at bottom, middle and the top regions of the building direction

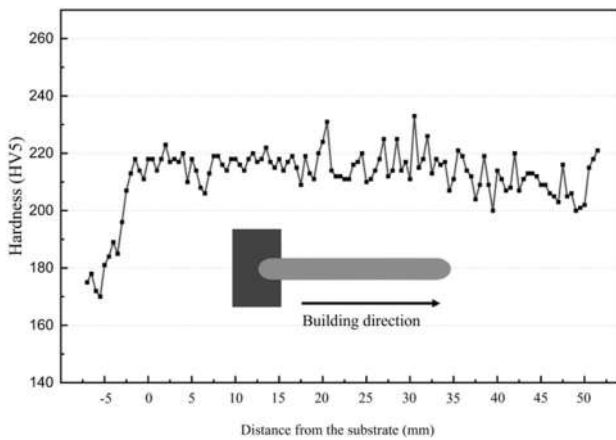
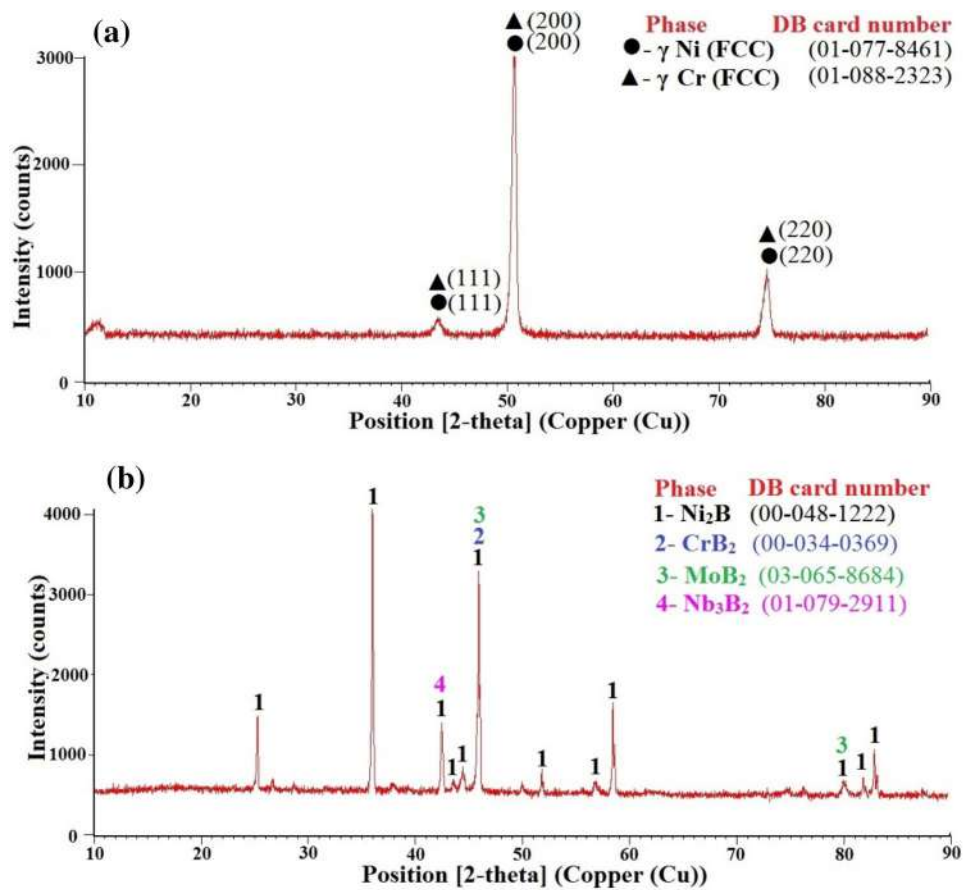


Fig. 4 Hardness distribution in the as- Arc-DED manufactured Inconel 625 wall structure along the building direction of 30 layers

transform from the cellular structure to elongated dendrites, as well as grain growth. This, in turn, causes a decrease in hardness. On the other hand, it can be seen by XRD analysis (Fig. 5) that this situation does not cause a phase change. Similarly, Jiang et al. [45] proposed that the temperature gradient of the liquid molten pool at the top of the sample gradually decreases. That is, as you move away from the substrate, the cooling rate slows down and the growth of the grain occurs which in turn causes a decrease in hardness, since the energy of the arc is continuous and increases the temperature of the component produced as a result of its accumulation in the sample.

XRD patterns of the as-Arc-DED manufactured and as-Arc-DED-manufactured + boronized Inconel 625 samples are shown in Fig. 5a, b, respectively. As seen in Fig. 5a, it was determined that the as-produced sample consisted only of γ nickel–chromium based solid solution (01-077-8461 and 01-088-2323) phase with FCC crystal structure. γ peaks obtained corresponding to 43.29 (111), 50.65 (200), 74.52 (220) degrees and planes and are in agreement with previous

Fig. 5 XRD pattern obtained on the surface of **a** as-Arc-DED manufactured Inconel 625, and **b** as-Arc-DED-manufactured + boronized Inconel 625 samples



studies produced with additive manufacturing in the literature. As can be seen in Fig. 5b after boronizing, the phase structure has completely changed and in accordance with the chemical content of Inconel 625 and the boron diffusion process applied, it has been determined that the dominant phase is Ni_2B , as well as the CrB , MoB and NbB phases are formed as minor phases. The dominant phase is Ni_2B with an angle of 35.98° and the orientation plane being (200).

Due to the low Fe contents in the produced samples, Fe-B phases did not form. In addition, oxide formation was not observed during boriding, since the boronizing crucibles are geared and ecrit Al_2O_3 powder is used on the surface of the boronizing powder, which avoids the contact with oxygen [32]. There is no study on Inconel 625 alloy produced by additive manufacturing and then subjected to boronizing process in open literature to compare with the current study. However, the phases obtained are in good agreement with the phases observed in the borided wrought Inconel 625 [29, 46, 47]. For example, Petrova et al. determined Ni_2B , Ni_3B_4 and Ni_3B phases in the structure as a result of boronizing of Inconel 625 alloy in $\text{B}_4\text{C} + \text{KBF}_4$ environment and reported that the hardness value of the boride layer was 2400 HV [46]. Similarly, Linder et al. obtained a coating layer consisting of boride and silicide phases (Ni_4B_3 , Ni_2B

and $\text{Ni}_6\text{Si}_2\text{B}$) with a hardness in the range of 1871–1994 HV as a result of boronizing the Inconel 625 alloy obtained by the HVOF method with EKKabor 2 powder (Si containing) [47]. In addition, Günen and Kanca reported that Ni_2B , NiB , CrB and Fe_2B phases were formed in the coating layer of the boronized wrought Inconel 625 alloy [29]. Therefore, it can be said that similar boride layers to those reported for the borided wrought Inconel 625 alloys were obtained in the borided Inconel 625 alloy specimens fabricated by Arc-DED in the current study.

Figure 6 shows the SEM micrograph of as-fabricated (untreated) Inconel 625 alloy by Arc-DED. This figure shows the microstructure in the longitudinal cross-section of the as-fabricated Inconel 625 alloy deposited by the Arc-DED process using GMAW.

In the production of the sample with the Arc-DED process, thirty layers were deposited with the height of each layer 6.5 mm, therefore, the specimen displayed a layered appearance. In the detailed microstructural examinations conducted on the sample, it was determined that there were no defects such as inter-layer cracks between the base layer and the substrate or pores, and that it had an appearance resembling a dendritic structure. Indeed, Abe and Sasahara reported that the dendritic growth direction is dependent on

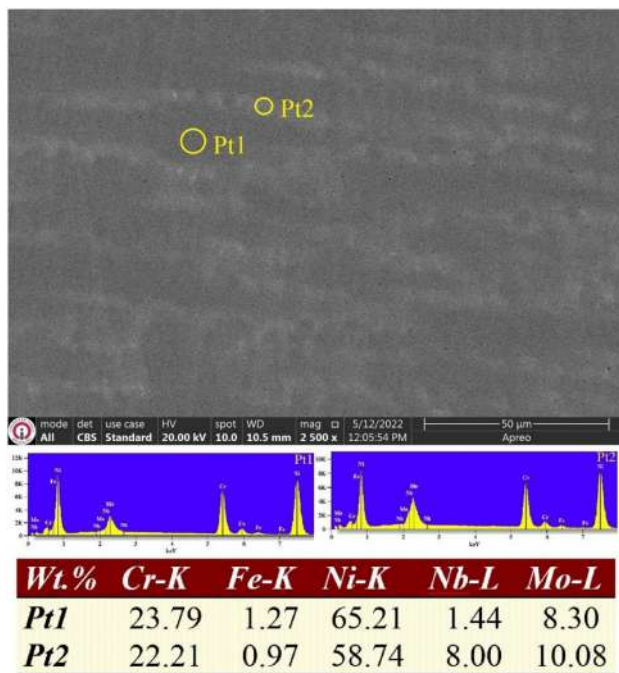


Fig. 6 SEM micrograph of the as-fabricated (non-borided) Inconel 625 alloy by Arc-DED

the direction of heat flow and is mostly perpendicular to the substrate [48]. Yangfan et al. attributed this to the tendency of the grains to grow preferably in the opposite direction of the heat flow to follow the maximum temperature gradient [44]. As the EDS analyzes taken from the dendritic and interdendritic regions shown by the SEM micrograph in Fig. 6 indicate, it was observed that the Nb and Mo contents of the interdendritic region were higher than the dendritic region, and the Ni, Cr, and Fe ratios were close to each other in these two regions. De Sousa Malafaia et al., stated that these regions may be M_6C particles according to the EDS results they obtained in their study where they examined the isothermal behavior of Inconel 625 alloy produced by casting, but they also pointed out that a definite judgment could not be made since these structures were not detected by XRD analysis [49].

The SEM micrograph of cross-section of boronized Arc-DED manufactured Inconel 625 specimen is illustrated in Fig. 7. When the cross-sectional microstructure view of the boronized Arc-DED manufactured Inconel 625 alloy is examined, the existence of three different regions on the surface is clearly seen. These regions are (i) 50 μm thick boride layer, (ii) 20 μm thick transition zone, and (iii) matrix structure consisting of dendritic and interdendritic regions as in the untreated Arc-DED Inconel 625 sample. It has been determined that the formed boride layer has a flat-uniform structure and it is free from any defects such as cracks, porosity and discontinuity. A diffusion zone consisting of

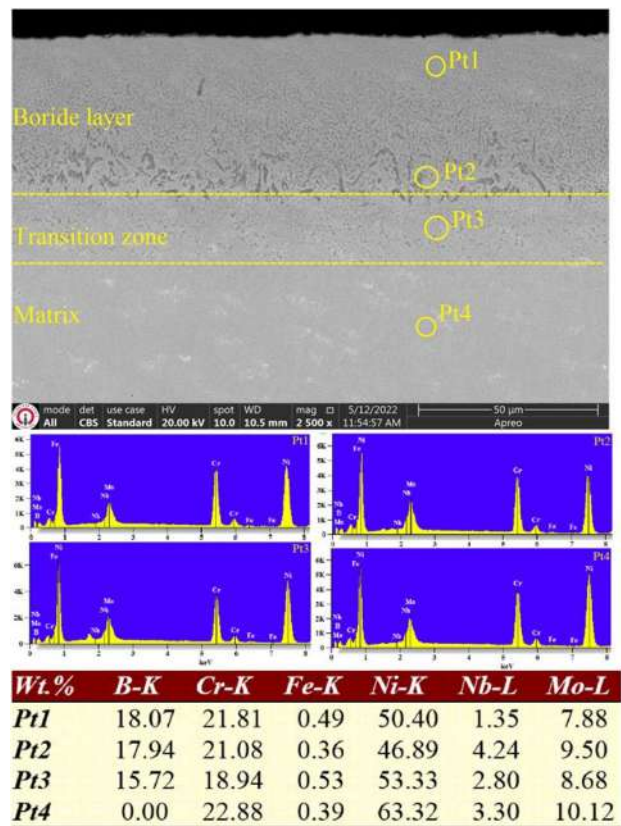


Fig. 7 The SEM micrograph of cross-section of boronized Arc-DED fabricated Inconel 625 specimen

alloying elements of the matrix of boron element was also observed under the boride layer. While the boron content near the upper surface of the nickel boride layer was wt.% 18, the boron ratio in the region close to the transition part decreased by 17 wt.%, however, an increase in the Nb and Mo ratios was detected in this region. In the part called the transition zone, the boron ratio is around 15 wt.%, while it is 0 wt.% in the matrix. Therefore, as in the previous studies published on superalloys, there was a gradual decrease in boron ratios throughout the depth of the boride layer and it reached zero to the substrate as stated by Campos-Silva et al. [31]. In contrast, the chromium content decreased by 21 wt.% in the boride layer and gradually decreased to 18 wt.% in the diffusion zone, while in the matrix it reached a value of ~23% by weight, as in the non-boronized material. Nb and Mo ratios are relatively low in the boride layer compared to the matrix. This is the result of the higher formation enthalpy of NbB and MoB phases than NiB and CrB. It is very important that the boride layers obtained on WAAM samples are homogeneous and dense, like the boride layers obtained on wrought Inconel 625 alloys. Because Kayali et al. [50] reported that the boride layers on the Inconel 718 produced by the electro-spark deposition (ESD) method

and subsequently boronized had lower hardness values than the boride layers obtained on the wrought Inconel 718. The authors attributed the lower hardness values to the oxide residues in the samples produced by the ESD method. A similar situation has also been reported in the boronizing of metal compacts produced by powder metallurgy (PM), and the lower hardness values of the boride layers were attributed to their oxide and porosity contents [51–53]. In studies carried out with ESD and PM, it has been reported that this will result in less improvement in wear resistance.

Considering the condition of the substrate after boronizing, the chemical content detected in the EDS analysis taken from the Pt4 region of Fig. 7 and the percentages of the elements detected in the Pt1 and Pt2 regions of Fig. 6 are close to each other. This is an indication that boriding process does not cause any negative effects on the substrate.

The surface condition of the boride layer is also as important as its cross-sectional area. Because, the first contact takes place via the surface in the conditions of wear, corrosion, etc. SEM surface micrographs and EDS analysis of the surface of the samples produced with Arc-DED and then borided are presented in Fig. 8.

When the surface of boride coatings is examined; it has been observed that most of the surface consists of $\sim 5 \mu\text{m}$ grains with angular geometry and $\sim 1 \mu\text{m}$ pits between these grains (Fig. 8a). When the higher magnification SEM micrograph was examined, pit formations were observed more clearly (Fig. 8b). These are related to the crystal structure of the boride phase, which varies depending on the boron–metal ratio in the structure of the boride coatings. Zhao et al., explains this as changes in the B/M ratio reveal domains of diverse and broad phase stability whose structures are largely based on close packing of metal atoms with boron atoms filling octahedral spaces [54]. Therefore, these structures are thought to exhibit a complex structure depending on the mixture of bonds between the transition metal and boron atoms. Consequently, in mixed-phase areas, the two phases present often precipitate in certain morphologies, allowing the microstructure to have a significant effect on the strength and fracture properties of the boride. In the EDS analysis conducted (Pt3), it was determined that 47.97% B and 50.56% Ni were present, while the O_2 ratio was found to be “0”. On equiaxial grains, the B ratio is 28.67, while the Ni ratio is 68.43. The fact that boron was detected at the rate of 69% in the pit regions gives the impression that boronizing powders remain in these pit regions, since the boronizing process is carried out in a solid environment.

The microhardness of Arc-DED manufactured Inconel 625, which was used as the substrate material, and subjected to normalization process, was determined to be 2.2 ± 0.1 GPa. On the other hand the hardness of boronized Arc-DED manufactured Inconel 625 increased up to 20.42 ± 0.8 GPa in the surface (boride layer), but this hardness gradually

decreased to 6.44 ± 0.84 GPa in the transition zone and 4.24 ± 0.33 GPa hardness in the matrix and hardness of boronized Arc-DED manufactured samples was higher than the samples non-boronized. The higher hardness of the boronized sample compared to the non-boronized sample can be attributed to the fact that the voids, oxide islands, etc. residues in the structure were improved by a secondary heat treatment. When the surface roughness values were examined, it was determined that the surface roughness of Arc-DED manufactured Inconel 625 sample was $0.59 R_a$ and the R_a value increased to 0.69 after boronizing. This is the result of pits formed between the grains in a structure consisting of grains with angular geometry as seen in Fig. 8.

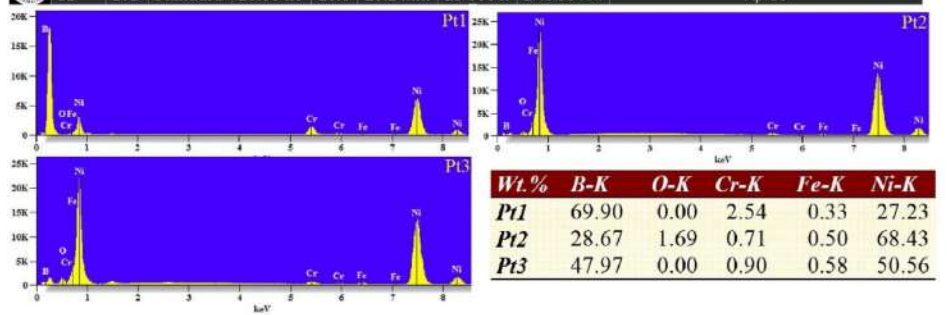
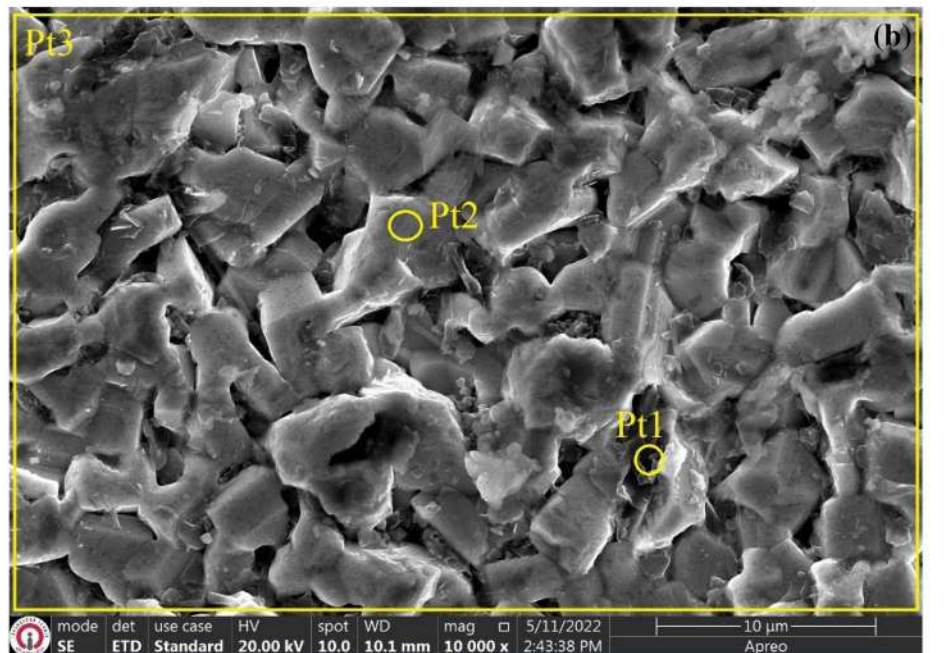
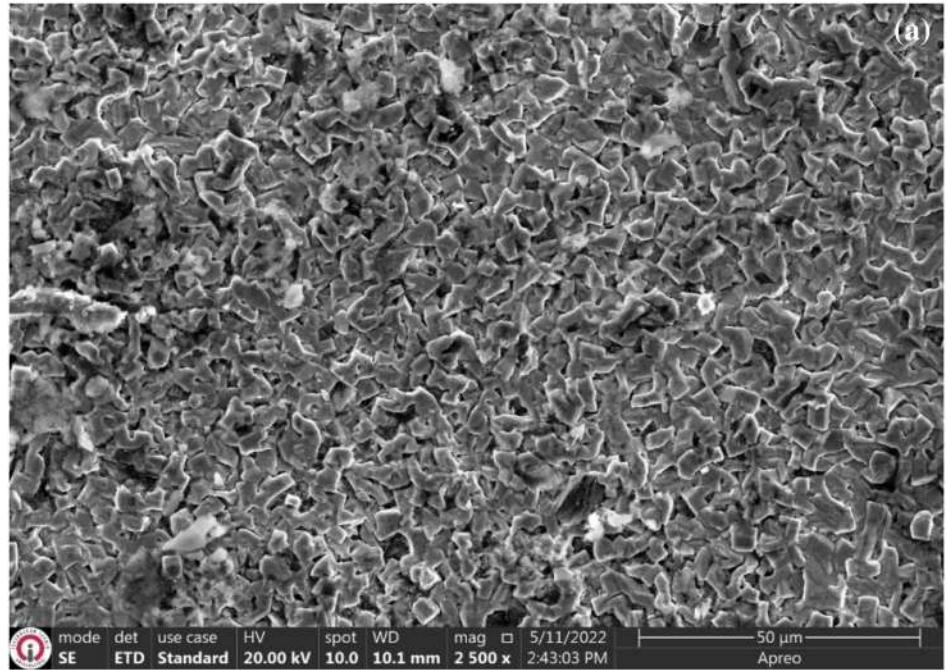
3.2 Friction and wear behavior

The wear test results of wrought Inconel 625, as- Arc-DED fabricated Inconel 625 and Arc-DED manufactured + boronized Inconel 625 samples at room temperature and 500°C are given in Fig. 9 as a function of sliding distance.

It can be seen from the friction coefficient (COF) graphs obtained from the wear tests carried out at room temperature that the non-boronized samples immediately reached the 0.85 level at the beginning of the test (5–10 m), and the friction remained stable for the remaining distance of the test, and both the wrought Inconel 625 and the non-boronized as-Arc-DED manufactured fabricated Inconel 625 samples followed a similar coefficient of friction course. The only difference between the friction coefficient courses of wrought Inconel 625 and non-boronized Arc-DED manufactured Inconel 625 samples is that the deviations in the friction course of the non-boronized as- Arc-DED fabricated Inconel 625 sample are higher. It is thought that this is due to the fact that the homogeneity of the additive structure created in the Arc-DED process is slightly low depending on the arc length. Tripathy et al. attributed less fluctuation in the friction coefficient of the wrought material to the increase in the wrought material conformity, making the contact more compliant, thereby reducing the local pressure and thus reducing the resistance to movement and subsequently reducing the deformation (slip) [55].

In the Arc-DED + boronized Inconel 625 sample, on the other hand, it was determined that the stable friction coefficient course was reached at the end of the 50 m wear distance and a course of 0.65 was observed in the rest of the test. A slight increase after 60 m is remarkable in the graphs of the CoF of both boronized and non-boronized samples at room temperature. Jeyaprakash et al. reported that an increase in the coefficient of friction (CoF) occurred as a result of the decrease in the adhesion resistance of the substrate as a result of the local increase in the temperature

Fig. 8 SEM micrograph of the surface of the boronized Arc-DED manufactured Inconel 625: **a** 2500X and **b** 10000X



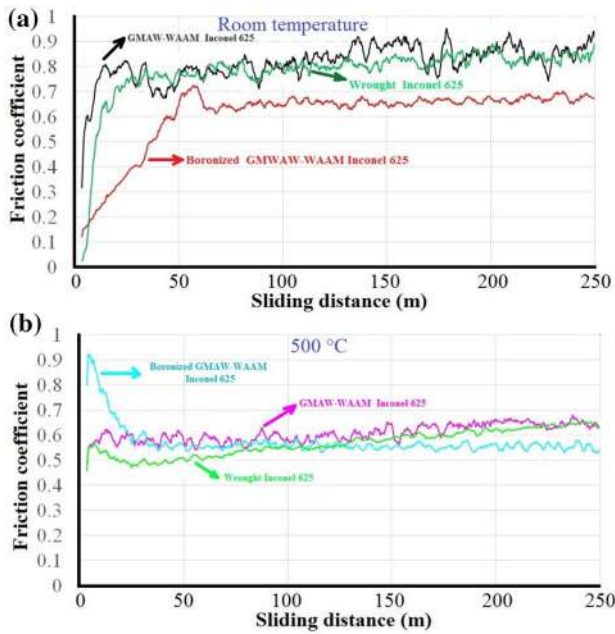


Fig. 9 COF graphs were obtained as the articulation against WC–Co ball: **a** room temperature and **b** 500 °C

between the contact points due to the increase in the sliding distance [56].

As seen in Fig. 8a, it can be observed that the CoF of the boronized sample is lower than that of the non-boronized samples. This is due to the fact that the surface has been hardened 10 times more as a result of boronizing. As a matter of fact, it has been stated by many scientists that the sink of abrasive ball into a harder surface will be more difficult than a relatively softer surface [32, 57, 58]. Moreover, the boride layers have self-lubricating properties. This makes CoF regimens generally lower [41].

When the friction coefficient data of the samples measured in the wear tests performed at 500 °C were examined (Fig. 9b), it was seen that lower friction coefficient values were obtained for both boronized and non-borided samples compared to room temperature. This situation can be attributed to the rapid oxidation of the surfaces due to the fact

that the wear processes are carried out at high temperatures and the lubricating effect of the oxide layer. A similar situation was obtained in the study of Feng et al. in which they investigated the wear mechanism of laser cladded Inconel 625 alloy at high temperatures and the authors attributed this to the occurrence of the abrasive wear mechanism at room temperature while adhesive wear mechanism takes place at high temperatures [59].

On the other hand, non-boronized samples showed an increasing trend in the CoF at the start of the test from 0.55 to 0.63, while in the boronized sample it started from 0.9 and reached the level of 0.58 with a rapid decrease at a distance of 25 m and followed a downward trend toward 0.53 in the rest of the test. The fact that the surface is hard, sharp and rough (Fig. 9a) in the initial stage of the test in the boronized sample causes a higher CoF. When the surface roughness is removed and a lubricating layer is formed on the surface, it has ensured that the friction coefficient is low on smoother surfaces. The lower CoF values obtained in both room temperature and high-temperature wear tests in the boronized sample are due to the microstructure, that is, the presence of hard boride phases in the microstructure. Because hard phases intensify crack formation and reduce crack diffusion rate. As a matter of fact, the SEM micrograph taken from the surface of the boronized sample after the room temperature abrasion test supports this claim.

In Table 5, the wear track widths and wear track depths observed in the wrought Inconel 625, as- Arc-DED fabricated Inconel 625 and Arc-DED manufactured + boronized Inconel 625 samples after the room temperature and 500 °C temperature dry sliding wear behavior analysis and the subsequently calculated wear trace volume and wear rates are given.

From Table 5, it was seen that the wear trace widths and depths formed on the surface of the boronized sample after both room temperature and 500 °C wear tests were lower, thus indicating that less wear damage occurred at both temperatures. Thanks to the 10 times harder boride layer formed on the surface by the boronizing process, the boronized samples showed 58.17 times and 3.86 times better abrasion resistance than the non-boronized samples in the tests

Table 5 Data obtained as a result of the ball-on-disc wear tests

Nomenclature	Wear temperature (°C)	Mean COF	Wear track width (μm)	Wear track depth (μm)	Volume loss (10^{-2}mm^3)	Wear rate ($10^{-5}\text{mm}^3/\text{Nm}$)
Wrought	25	0.78 ± 0.05	1372 ± 65	56 ± 3.2	183.24 ± 9.2	73.30 ± 3.2
Arc-DED		0.81 ± 0.05	1427 ± 66	50 ± 3.4	168.22 ± 8.5	67.29 ± 2.9
Boronized		0.61 ± 0.03	309 ± 14	4.33 ± 0.4	3.16 ± 0.1	1.26 ± 0.05
Wrought	500	0.58 ± 0.04	1175 ± 57	41 ± 2.9	112.59 ± 6.2	45.03 ± 2.1
Arc-DED		0.61 ± 0.05	1066 ± 53	35 ± 2.6	87.83 ± 4.3	35.13 ± 1.5
Boronized		0.57 ± 0.03	714 ± 32	17 ± 1.7	29.15 ± 1.0	11.66 ± 0.4

performed at room temperature and 500 °C, respectively. This is the case where, according to Archard's wear law, the mass loss is inversely proportional to the hardness of the material, and this is in line with the findings of the study performed by Jeyaprakash et al. [56] and Gonzales et al. [60].

The eroded surface morphology of the samples subjected to ball-on disc abrasion treatment at room temperature is shown in Figs. 10, 11, 12. Similar wear marks were observed on the surface of both non-boronized as- Arc-DED fabricated Inconel 625 (Fig. 10) and non-boronized as-GMAW-WAAM fabricated Inconel 625 (Fig. 11) materials, and there are wear residues and irregular parts on the worked surfaces of the samples due to shear stresses. Because continuous sliding causes shear stresses on the abraded surfaces. As a matter of fact, it has been suggested by Birol [61] that shear stresses cause plastic deformation after a certain stage and produce plate-like parts on the surface, and consequently by repeatedly producing plate-like morphology, it will lead to the presence of wear debris and irregular parts on the surface. When Figs. 10 and 11 are examined, it is clearly seen that there are traces of plastic deformation on the surface and traces of grooving in some areas. Thomas and Tait [62] argue that this is indicative of the higher plastic deformation and less wear resistance to abrasion observed in samples with low hardness. Therefore, it was concluded that the wear mechanisms observed in the unbored samples are micro-grooving, deep grooves, abrasive and severe plastic deformation. These findings are in agreement with the coefficient of friction plots obtained at room temperature in which high frictional forces observed. And the high friction force causes high plastic deformation and serious damages. EDS analyzes performed on the sample surface after the wear test showed that the presence of O₂ in the non-boronized samples was close to "0". This confirms the high oxidation resistance of superalloys. Therefore, when the wear morphologies were examined, it was determined that abrasive and plastic deformation were more dominant than other mechanisms on the non-boronized worn surfaces, and the findings were consistent with the findings of Radu and Li's study [63] on Stellite 21 alloy.

When the wear trace appearance of the boronized sample is examined (Fig. 12a), a much narrower and shallower wear trace formation was observed compared to the non-boronized samples, and the data in Table 5 supports this point.

SEM images of the worn surface of the boronized sample in Fig. 12b show that micro-cracks and local fractures occur on the surface. As a result of the 20 N load applied to the hard boride layer in these samples, the abrasive ball could not easily penetrate the hard surface, causing micro-cracks on the surface due to the repeated loads applied. In addition, boron's high affinity for oxygen led to the formation of an oxide layer on the surface. The resulting oxide layer

resulted in a lower coefficient of friction and, as a result, less wear damage. As a matter of fact, as seen in the EDS analyzes of the samples, high rates of boron (37–45% wt.) and oxygen (wt. 8–13%) were detected on the surface of the material. Therefore, the wear mechanism of boronized samples at room temperature was considered to be micro-crack and oxidative.

When the SEM images (Figs. 13, 14, 15) taken from the surface of the samples after the wear tests performed at 500 °C are examined, it is seen that, contrary to the obvious wear lines seen in the room temperature traces of the non-boronized samples (Figs. 10 and 11), the appearance of the surface morphology with relatively smooth regions with oxidation in places, which is formed by the compression of the wear residues held in contact between the substrate and the ball, draws attention. Tripathy et al. explains this as a result of the fact that the glazed oxide layer, which very firmly adheres to the substrate, acts as an intermediate protective layer between the abrasive ball and the substrate when sufficient contact pressure is applied at high temperatures [55]. This glazed layer reduces direct contact with the substrate and reduces excessive wear. It was determined that the wear track width and depth of the unbored specimens at room temperature were lower than 500 °C, so the wear volume losses were lower (Table 3). The observation of lower wear of non-boronized samples at elevated temperatures compared to room temperature is in line with the findings of Iwabuchi [64] and Tripathy et al. [55]. The case that superalloys are subject to lower volume losses than room temperature due to the oxide layer formed on their surfaces in high-temperature wear processes has also been reported by Radu and Li [63], Stott [65], and Rahman et al. [66]. Glazed layer tribological behavior was first determined by Iwabuchi [64] for wrought Inconel 625, and many authors have reported that it is also observed in the wear behavior of other nickel-based alloys [32, 61, 63, 66–69].

In tests carried out at 500 °C, the oxidation rate becomes much higher than at room temperature due to the effect of heat and the presence of sufficient air in the environment and the formation of an oxide layer on nickel-based alloys. High levels of Ni, Cr and O₂ were detected in this upper layer, as seen in the EDS analysis, and it was concluded that this layer was composed of nickel oxide and chromium oxide. Findings similar to the oxide layer formed in wear tests performed at high temperatures, was also observed by Rahman et al. in high-temperature wear tests of Inconel 617 and Incoloy 800HT alloys [66, 69].

The surface appearance of the boronized sample after the abrasion process at 500 °C, on the other hand, has a wider abrasion trace width compared to room temperature, but the surface consists of a completely smooth surface and there are wear residues in places. The formation of a wider trace than the room temperature is the result of the rapid oxidation of the

Fig. 10 SEM micrographs and EDS point analysis of the worn surface of wrought Inconel 625 exposed to wear testing at room temperature: **a** 150X and **b** 1000X

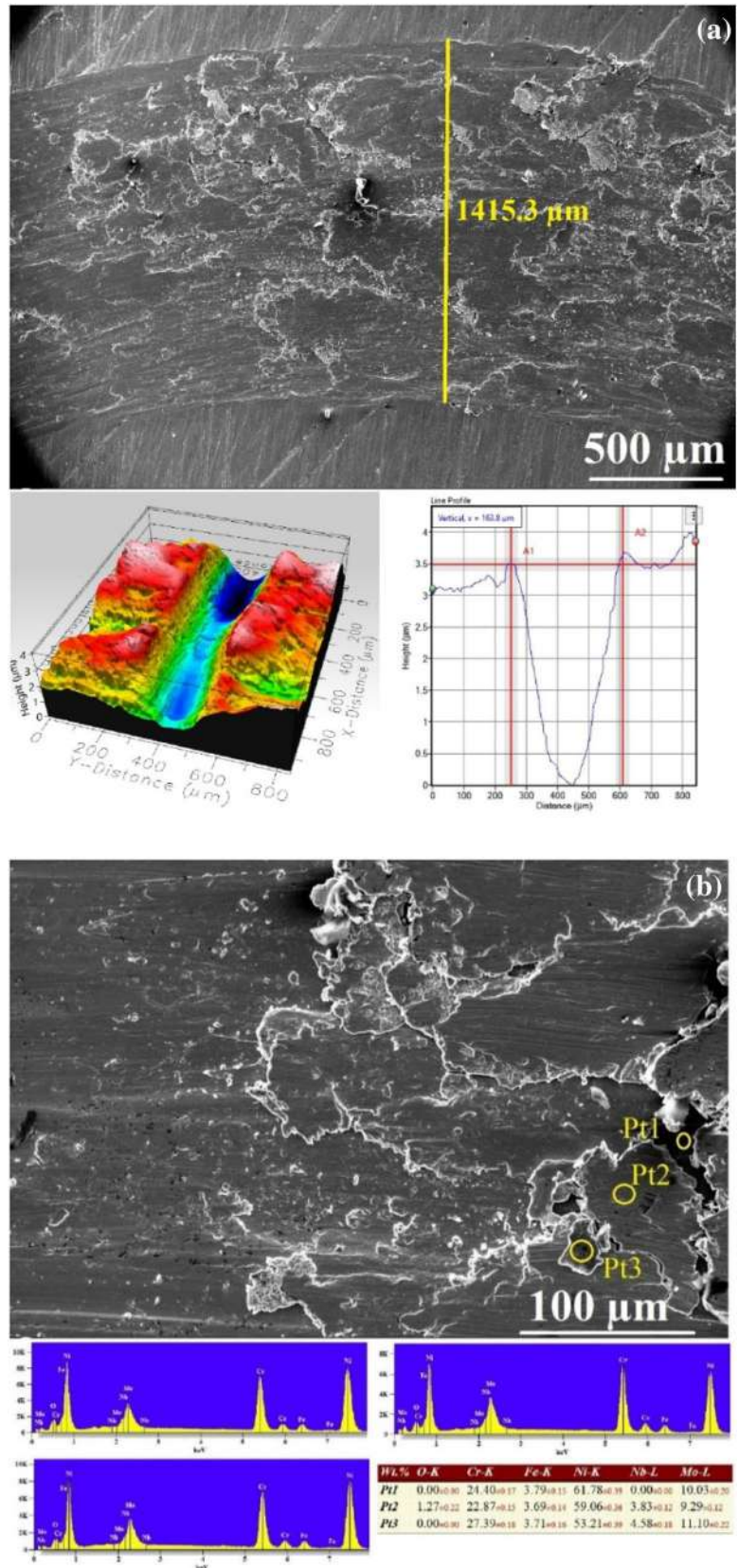


Fig. 11 SEM micrographs and EDS point analysis of the worn surface of non-boronized as Arc-DED manufactured fabricated Inconel 625 Ni-based superalloy exposed to wear testing at room temperature: **a** 150X and **b** 1000X

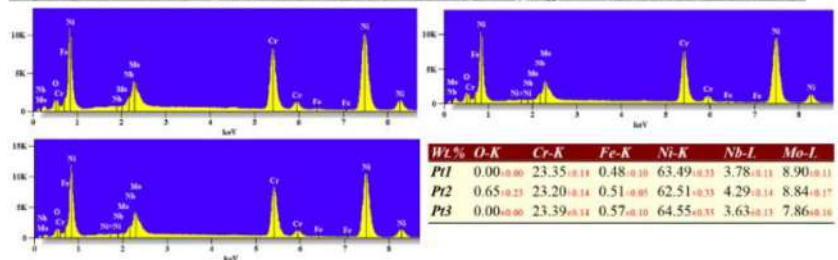
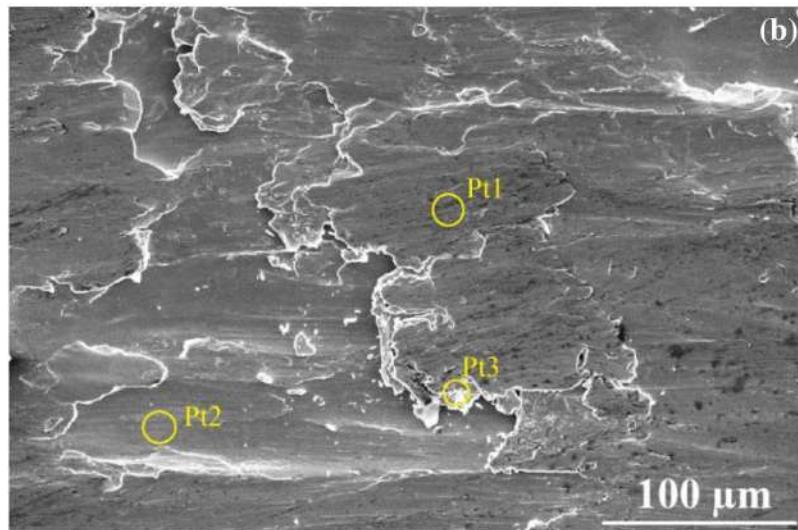
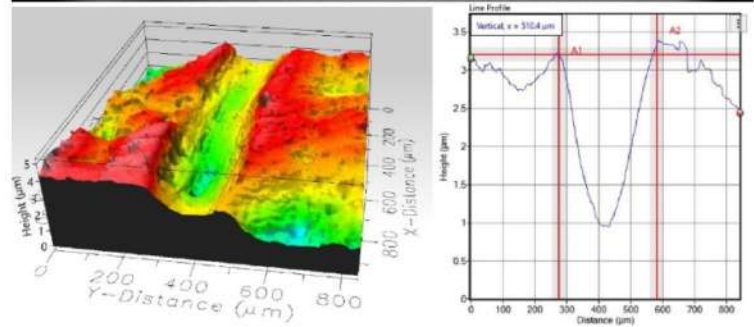
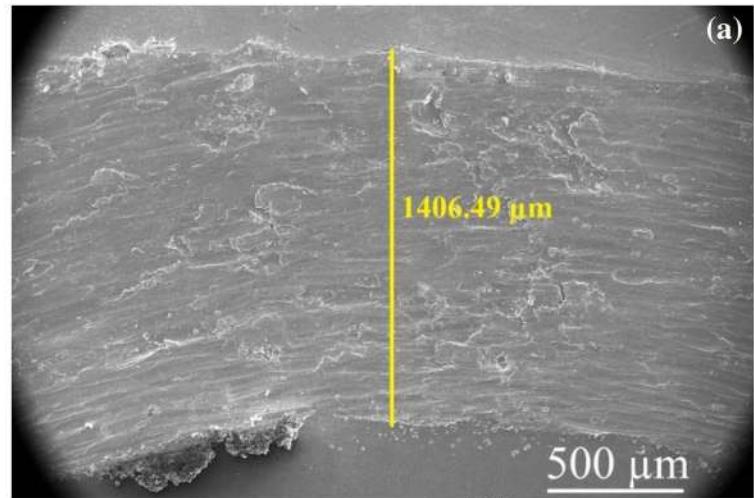
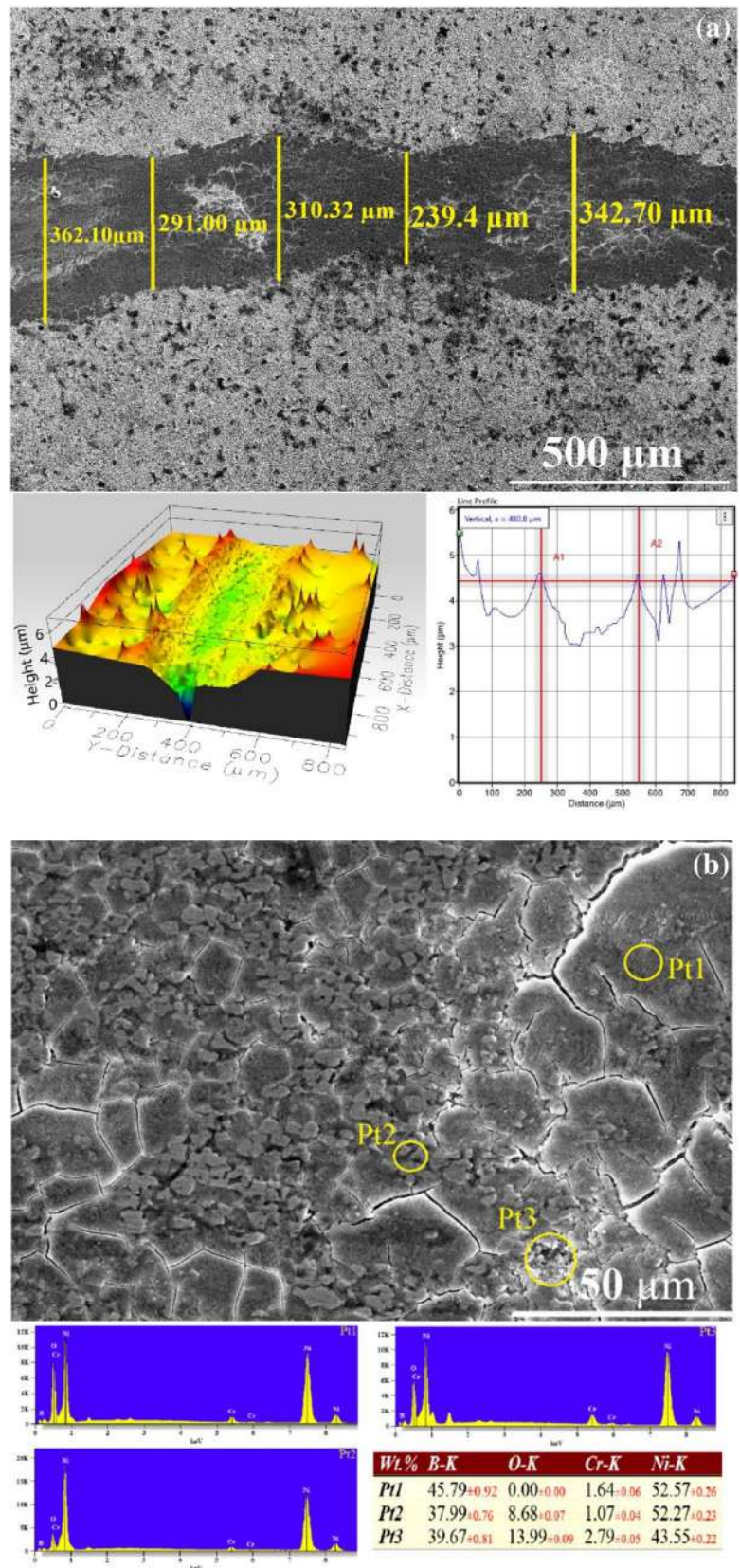


Fig. 12 SEM micrographs and EDS point analysis of the worn surface of Arc-DED manufactured + boronized Inconel 625 specimen exposed to wear testing at room temperature: **a** 250X and **b** 2500X



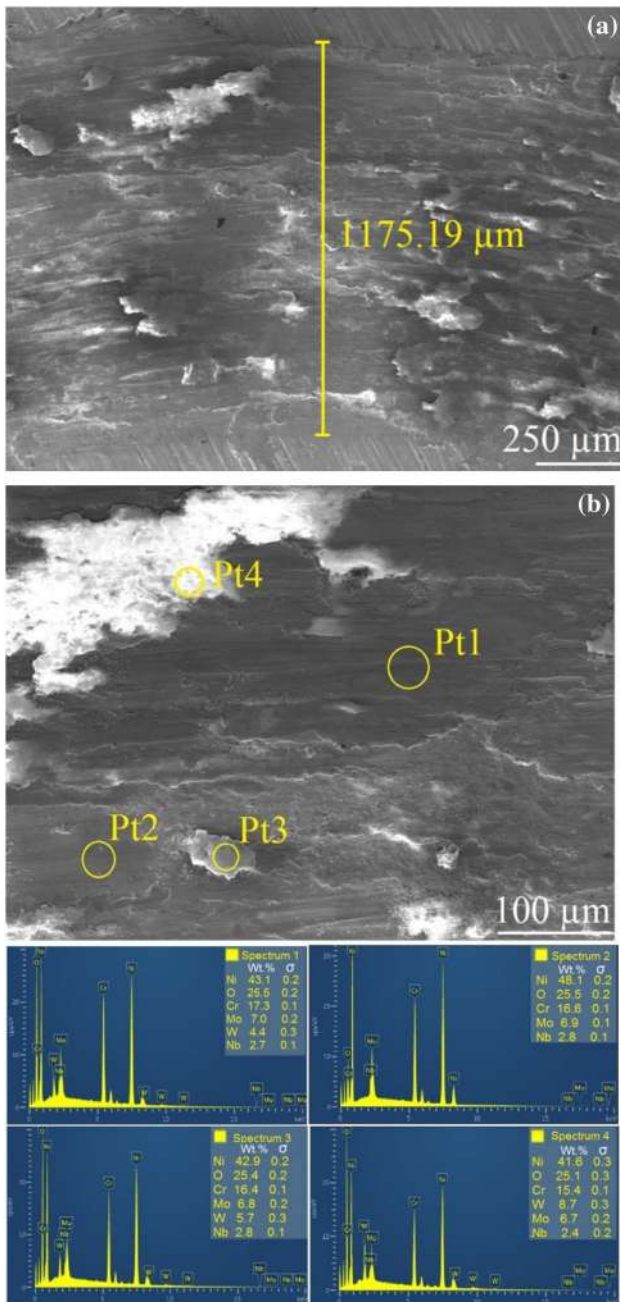


Fig. 13 SEM micrographs and EDS point analysis of the worn surface of wrought Inconel 625 exposed to wear testing at 500 °C: **a** 150X and **b** 1000X

boride layer, which has a high affinity for oxidation, with the temperature, and the loss in the mechanical properties of the boride layer. As a matter of fact, O₂ rates are around 60–65% wt as seen from the EDS analysis. When evaluated in terms of wear mechanism, it was concluded that oxidation supported polishing type wear mechanism is the dominant mechanism at

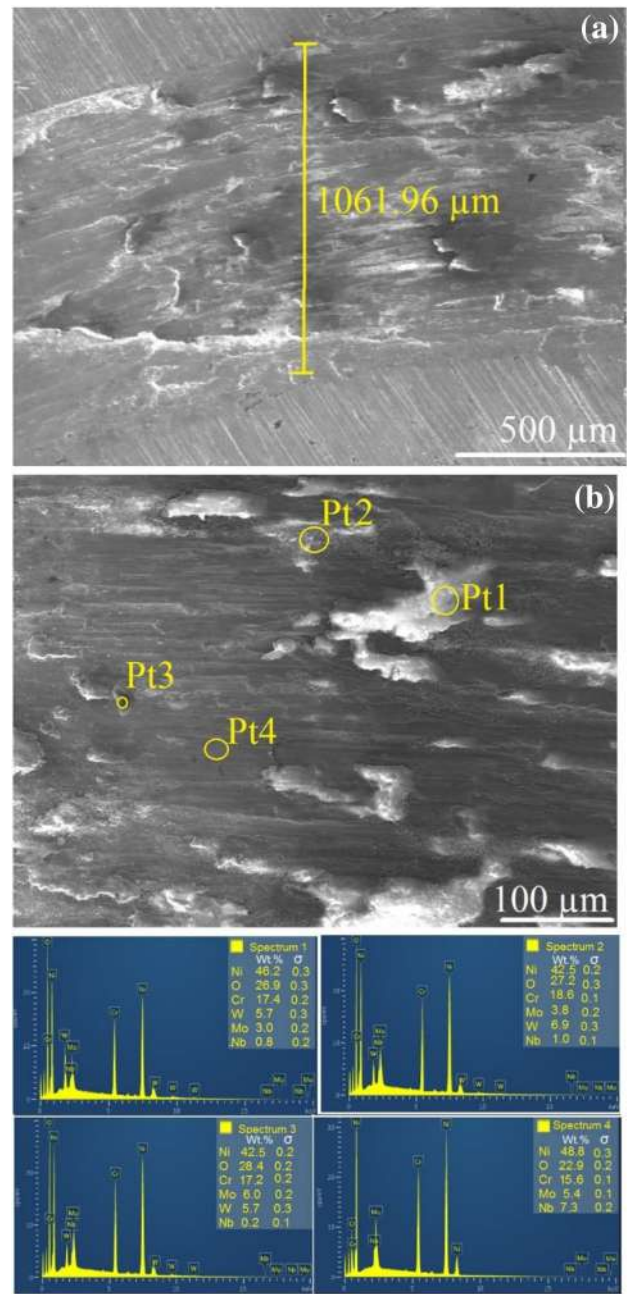


Fig. 14 SEM micrographs and EDS point analysis of the worn surface of non-boronized as Arc-DED fabricated Inconel 625 superalloy exposed to wear testing at 500 °C: **a** 150X and **b** 1000X

high-temperature wear of borided Arc-DED-produced Inconel 625. These findings are consistent with the observations in high-temperature wear behavior of boronized Inconel 718 and boronized Monel 400 alloys by Günen [32] and Küçük et al. [70], respectively.

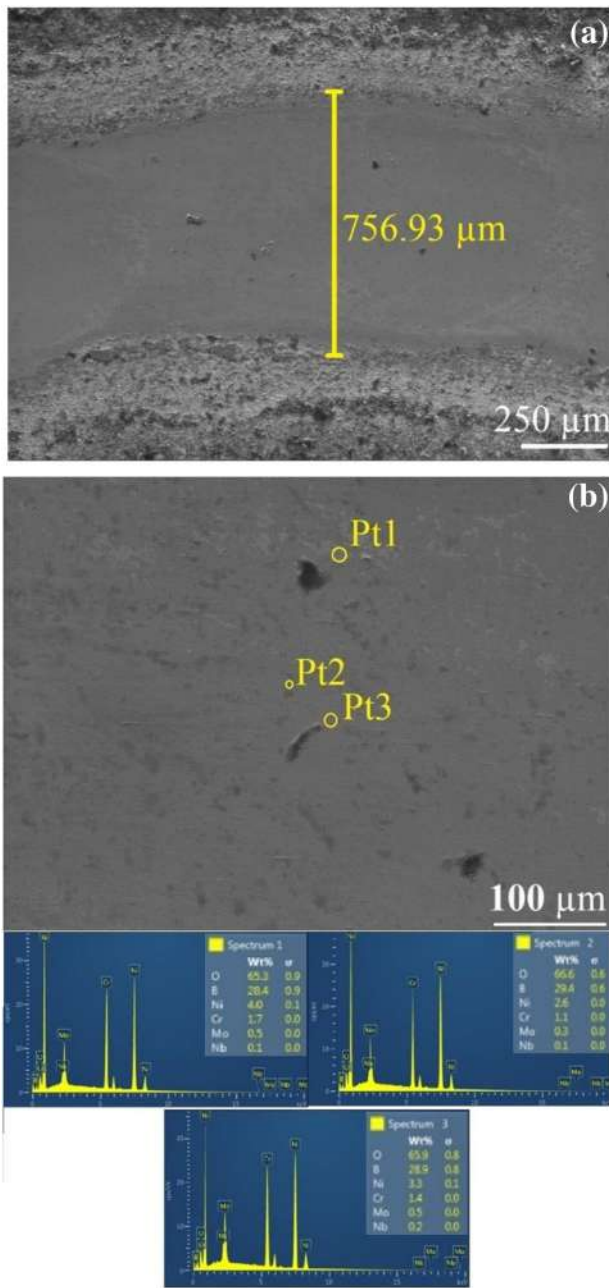


Fig. 15 SEM micrographs and EDS point analysis of the worn surface of Arc-DED manufactured + boronized Inconel 625 specimen exposed to wear testing at 500 °C: **a** 150X and **b** 1000X

4 Conclusions

In this study, boronizing and homogenization heat treatment was applied simultaneously at 980 °C for 1 h in order to improve the microstructure, hardness and wear resistance of Ni-based superalloy Inconel 625 samples produced by the Arc-DED method. The results and important findings are briefly summarized below:

Inconel 625 alloy samples were successfully fabricated by the Arc-DED process without various defects such as dividing lines, porosity, irregularly shaped oxide, voids and cracks. The surface of the wall structure has a rough structure due to the spherical mass transfer mechanism involved in the Arc-DED process.

The chemical composition of the targeted Inconel 625 alloy has been achieved, and it has been determined that the phase structure of the fabricated Inconel 625 alloy samples has only a face-centered cubic (fcc) crystal structure as the case in wrought Inconel 625 alloys.

As a result of the boronizing process, a boride layer with a thickness of 50 μm and a hardness of 20 GPa was formed on the surface. Thanks to this layer, the surface hardness of Inconel 625 alloy wall structure fabricated by Arc-DED has been improved by 5 times.

It has been determined that the boride layer formed on the surface is mostly composed of Ni₂B phase, as well as a low percentage of CrB₂, MoB₂ and Nb₃B₂ hard boride phases.

The high affinity of boron toward oxygen provided the boronized samples with finely dispersed hard oxides to exhibit lower friction coefficient values at both room temperature and 500 °C than the non-boronized samples. Wear temperatures have an effect on the coefficient of friction of the Inconel 625. The mean friction coefficients of all Inconel 625 alloy samples tested, namely wrought Inconel 625, non-boronized as- Arc-DED-fabricated Inconel 625 and Arc-DED manufactured + boronized Inconel 625 samples, decreased with increasing temperature.

Arc-DED manufactured + boronized Inconel 625 samples showed 58.17 times better wear resistance at room temperature and 3.86 times better at 500 °C than non-boronized samples. The decrease in the improvement in wear rates at high temperatures is a result of the oxidation-induced reduction in Arc-DED manufactured + boronized samples, which is in contrast to the oxidation-induced improvement in non-boronized as- Arc-DED-fabricated samples.

The temperature had a significant effect on the wear mechanisms of the all worn samples. It is as follows: while the wear mechanism of the non-boronized samples was abrasive and delamination at room temperature, it turned into oxidation-assisted adhesion and plastic deformation at 500 °C. On the other hand, the wear mechanism of the boronized sample at room temperature was micro-crack and oxidative wear mechanism, and it turned into an oxidation-assisted polishing wear mechanism at 500 °C.

It can also be concluded that the improvement of room temperature and high-temperature wear resistance of the Arc-DED fabricated Inconel 625 parts by boronizing can expand the use of additively manufactured alloys in wear environments.

Finally, this work has demonstrated that the Arc-DED process can be a viable engineering manufacturing technology for Inconel 625 components with hard surfacing.

Data availability statement The data that support the findings of this study are available from the corresponding author upon reasonable request.

Declarations

Conflict of interest The authors declare no financial or commercial conflict of interest.

References

- Ikeo N, Fukuda H, Matsugaki A, Inoue T, Serizawa A, Matsuzaka T, Ishimoto T, Ozasa R, Gokcekaya O, Nakano T (2021) 3D puzzle in cube pattern for anisotropic/isotropic mechanical control of structure fabricated by metal additive manufacturing. *Crystals* 11:959. <https://doi.org/10.3390/cryst11080959>
- Smith J, Xiong W, Yan W, Lin S, Cheng P, Kafka OL, Wagner GJ, Cao J, Liu WK (2016) Linking process, structure, property, and performance for metal-based additive manufacturing: computational approaches with experimental support. *Comput Mech* 57(4):583–610. <https://doi.org/10.1007/s00466-015-1240-4>
- Kannan GB, Rajendran DK (2017) A review on status of research in metal additive manufacturing. In: *Advances in 3D printing & additive manufacturing technologies*. Wimpenny D, Pandey P, Kumar L (Eds), Springer, Singapore, pp. 95–100. https://doi.org/10.1007/978-981-10-0812-2_8
- Lui EW, Medvedev AE, Edwards D, Qian M, Leary M, Brandt M (2022) Microstructure modification of additive manufactured Ti-6Al-4V plates for improved ballistic performance properties. *J Mater Process Technol* 301:117436. <https://doi.org/10.1016/j.jmatprotec.2021.117436>
- Guler S, Serindag HT, Çam G (2022) Wire arc additive manufacturing (WAAM): Recent developments and prospects. *Eng Machin* 63(706):82–116. <https://doi.org/10.46399/muhendismakina.1085716>
- Wrobel R, Mecrow B (2020) A comprehensive review of additive manufacturing in construction of electrical machines. *IEEE Trans Energy Convers* 35(2):1054–1064. <https://doi.org/10.1109/TEC.2020.2964942>
- Sathies T, Senthil P (2021) A Review on Milestones Achieved in the Additive Manufacturing of Functional Components. *Advanced Materials and Manufacturing Processes*. CRC Press, Florida, USA, pp 135–154
- Camacho DD, Clayton P, O'Brien WJ, Seepersad C, Juenger M, Ferron R, Salamone S (2018) Applications of additive manufacturing in the construction industry - A forward-looking review. *Autom Constr* 89:110–119. <https://doi.org/10.1016/j.autcon.2017.12.031>
- Ozer G (2020) A Review on Additive Manufacturing Technologies. *Niğde Ömer Halisdemir Üniversitesi Mühendislik Bilimleri Dergisi* 9(1):606–621. <https://hdl.handle.net/11352/3583>
- Bandyopadhyay A, Gualtieri T, Bose S (2016) *Global engineering and additive manufacturing*. In: *Additive Manufacturing*. Bandyopadhyay A and Bose S (Eds), CRC Press, Florida, USA
- Yang L, Hsu K, Baughman B, Godfrey D, Medina F, Menon M, Wiener S (2017) *Additive manufacturing of metals: The technology, materials, design and production*. Springer, Cham, Switzerland, pp 45–61
- Gouge M, Michaleris P (2017) *Thermo-mechanical modeling of additive manufacturing*. Butterworth-Heinemann, Elsevier, Netherlands
- Fang L, Cheng L, Glerum JA, Bennett J, Cao J, Wagner GJ (2022) Data-driven analysis of process, structure, and properties of additively manufactured Inconel 718 thin walls. *npj Comput Mater* 8:126. <https://www.nature.com/articles/s41524-022-00808-5>
- Tofail SA, Koumoulos EP, Bandyopadhyay A, Bose S, O'Donoghue L, Charitidis C (2018) Additive manufacturing: Scientific and technological challenges, market uptake and opportunities. *Mater Today* 21(1):22–37. <https://doi.org/10.1016/j.mattod.2017.07.001>
- Gebhardt A, Hötter JS (2016) *Additive manufacturing: 3D printing for prototyping and manufacturing*. Carl Hanser Verlag GmbH & Company KG, Munich, Germany
- Derekar KS (2018) A review of wire arc additive manufacturing and advances in wire arc additive manufacturing of aluminium. *Mater Sci Technol* 34(8):895–916. <https://doi.org/10.1080/02670836.2018.1455012>
- Liu J, Xu Y, Ge Y, Hou Z, Chen S (2020) Wire and arc additive manufacturing of metal components: A review of recent research developments. *Int J Adv Manuf Technol* 111:149–198. <https://doi.org/10.1007/s00170-020-05966-8>
- Çam G (2022) Prospects of producing aluminum parts by wire arc additive manufacturing (WAAM). *Mater Today Proc* 62(1):149–198. <https://doi.org/10.1016/j.matpr.2022.02.137>
- Xia C, Pan Z, Polden J, Li H, Xu Y, Chen S, Zhang Y (2020) A review on wire arc additive manufacturing: Monitoring, control and a framework of automated system. *J Manuf Syst* 57:31–45. <https://doi.org/10.1016/j.jmsy.2020.08.008>
- Nagasai BP, Malarvizhi S, Balasubramanian V (2022) Mechanical properties and microstructural characteristics of wire arc additive manufactured 308L stainless steel cylindrical components made by gas metal arc and cold metal transfer arc welding processes. *J Mater Process Technol* 307:117655. <https://doi.org/10.1007/s13632-022-00841-2>
- Harris ID (2017) *Development and implementation of metals additive manufacturing*. Additive Manufacturing Handbook. CRC Press, Florida, USA, pp 215–224
- Çam G, Fischer A, Ratjen R, dos Santos JF, Koçak M (1998) Properties of Laser Beam Welded Superalloys Inconel 625 and 718. in *Proc. of 7th European Conference on Laser Treatment of Materials, ECLAT '98*, September 21–23, 1998, Hannover, Germany, ed. B.L. Mordike, pub. Werkstoff-Informationsgesellschaft mbH, Frankfurt, pp. 333–338.
- Çam G, Koçak M (1998) Progress in joining of advanced materials - Part II: Joining of metal matrix composites and joining of other advanced materials. *Sci Technol Weld Join* 3(4):159–175. <https://doi.org/10.1179/stw.1998.3.4.159>
- Çam G, Koçak M (1998) Progress in joining of advanced materials. *Int Mater Rev* 43(1):1–44. <https://doi.org/10.1179/imr.1998.43.1.1>
- Tanvir ANM, Ahsan MdRU, Ji C, Hawkins W, Bates B, Kim DB (2019) Heat treatment effects on Inconel 625 components fabricated by wire+ arc additive manufacturing (WAAM) - Part I: Microstructural characterization. *Int J Adv Manuf Technol* 103:3785–3798. <https://doi.org/10.1007/s00170-019-03828-6>
- Tanvir ANM, Ahsan MdRU, Seo G, Kim JD, Ji C, Bates B, Lee Y, Kim DB (2020) Heat treatment effects on Inconel 625 components fabricated by wire+ arc additively manufacturing (WAAM) - Part 2: Mechanical properties. *Int J Adv Manuf Technol* 110:1709–1721. <https://doi.org/10.1007/s00170-020-05980-w>
- Safarzade A, Sharifitabar M, Afarani MS (2020) Effects of heat treatment on microstructure and mechanical properties of Inconel 625 alloy fabricated by wire arc additive manufacturing process.

- Trans Nonferrous Metals Soc China 30:3016–3030. [https://doi.org/10.1016/S1003-6326\(20\)65439-5](https://doi.org/10.1016/S1003-6326(20)65439-5)
28. Gunes I, Kayali Y (2014) Investigation of mechanical properties of borided Nickel 201 alloy. *Mater Des* 53:577–580. <https://doi.org/10.1016/j.matdes.2013.07.001>
 29. Günen A, Kanca E (2017) Characterization of borided Inconel 625 alloy with different boron chemicals. *Pamukkale University J Eng Sci* 23(4):411–416. <https://doi.org/10.5505/pajes.2017.56689>
 30. Frackowiak M, Makuch N, Dziarski P, Kulka M, Taktak S (2018) Fracture toughness of plasma paste-borided layers produced on nickel-based alloys. In: *Advances in Manufacturing*, Hamrol A, Ciszak O, Legutko S, Jurczyk M (Eds), Lecture Notes in Mechanical Engineering, Springer, Cham, Switzerland, pp. 923–932. https://doi.org/10.1007/978-3-319-68619-6_89
 31. Campos-Silva I, Contla-Pacheco AD, Figueroa-López U, Martínez-Trinidad J, Garduño-Alva A, Ortega-Avilés M (2019) Sliding wear resistance of nickel boride layers on an Inconel 718 superalloy. *Surf Coat Technol* 378:124862. <https://doi.org/10.1016/j.surfcoat.2019.06.099>
 32. Günen A (2020) Properties and high temperature dry sliding wear behavior of boronized Inconel 718. *Metall Mater Trans A* 51(2):927–939. <https://doi.org/10.1007/s11661-019-05577-3>
 33. Makuch N, Dziarski P, Kulka M, Keddám M (2021) Growth kinetics and some mechanical properties of plasma paste borided layers produced on Nimonic 80A-alloy. *Materials* 14(18):5146. <https://doi.org/10.3390/ma14185146>
 34. Guroł U, Dilibal S, Turgut B, Koçak M (2022) Characterization of a low-alloy steel component produced with wire arc additive manufacturing process using metal-cored wire. *Mater Test* 64(6):755–767
 35. Bagherzadeh A, Koc B, Budak E, Isik M (2022) High-speed machining of additively manufactured Inconel 718 using hybrid cryogenic cooling methods. *Virtual Phys Prototyp* 17(3):419–436. <https://doi.org/10.1080/17452759.2022.2034081>
 36. Ravi G, Murugan N, Arulmani R (2020) Microstructure and mechanical properties of Inconel-625 slab component fabricated by wire arc additive manufacturing. *Mater Sci Technol* 36(16):1785–1795. <https://doi.org/10.1080/02670836.2020.1836737>
 37. Chintala A, Tejaswi Kumar M, Sathishkumar M et al (2021) Technology development for producing Inconel 625 in aerospace application using wire arc additive manufacturing process. *J Mater Eng Perform* 30:5333–5341. <https://doi.org/10.1007/s11665-021-05781-6>
 38. Wang YF, Chen XH, Su CC (2019) Microstructure and mechanical properties of Inconel 625 fabricated by wire-arc additive manufacturing. *Surf Coat Technol* 374:116–123. <https://doi.org/10.1016/j.surfcoat.2019.05.079>
 39. Contla-Pacheco AD, Keddám M, Lartundo-Rojas L, Ortega-Avilés M, Mejía-Caballero I, Campos-Silva I (2021) Application of the Heat Balance Integral Method to the growth kinetics of nickel boride layers on an Inconel 718 superalloy. *Surf Coat Technol* 420:127355. <https://doi.org/10.1016/j.surfcoat.2021.127355>
 40. Günen A, Kanca E, Demir M, Er Y, Sagam G, Gok MS (2017) Microabrasion wear behavior of fast-borided steel tooth drill bits. *Tribol Trans* 60(2):267–275. <https://doi.org/10.1080/10402004.2016.1159359>
 41. Kulka M (2019) Current trends in boronizing. Springer Nature Switzerland AG, Cham, Switzerland, pp. 17–98.
 42. Sezgin CT, Hayat F (2022) The effects of boronizing process on tribological properties and corrosive behavior of a novel high manganese steel. *J Mater Process Technol* 300:117421. <https://doi.org/10.1016/j.jmatprotec.2021.117421>
 43. Oliver WC, Pharr GM (2010) Nanoindentation in materials research: Past, present, and future. *MRS Bull* 35(11):897–907. <https://doi.org/10.1557/mrs2010.717>
 44. Yangfan W, Xizhang C, Chuanchu S (2019) Microstructure and mechanical properties of Inconel 625 fabricated by wire-arc additive manufacturing. *Surf Coat Technol* 374:116–123. <https://doi.org/10.1016/j.surfcoat.2019.05.079>
 45. Jiang Q, Zhang P, Yu Z, Shi H, Li S, Wu D, Yan H, Ye X, Chen J (2021) Microstructure and mechanical properties of thick-walled Inconel 625 alloy manufactured by wire arc Additive manufacture with different torch paths. *Adv Eng Mater* 23:2000728. <https://doi.org/10.1002/adem.202000728>
 46. Petrova RS, Suwattananont N, Samardzic V (2008) The effect of boronizing on metallic alloys for automotive applications. *J Mater Eng Perform* 17(3):340–345. <https://doi.org/10.1007/s11665-008-9228-2>
 47. Lindner T, Löbel M, Hunger R, Berger R, Lampke T (2020) Boronizing of HVOF-sprayed Inconel 625 coatings. *Surf Coat Technol* 404:126456. <https://doi.org/10.1016/j.surfcoat.2020.126456>
 48. Abe T, Sasahara H (2016) Dissimilar metal deposition with a stainless steel and nickel-based alloy using wire and arc-based additive manufacturing. *Precis Eng* 45:387–395. <https://doi.org/10.1016/j.precisioneng.2016.03.016>
 49. De Sousa Malafaia AM, de Oliveira RB, Latu-Romain L, Wouters Y, Baldan R (2020) Isothermal oxidation of Inconel 625 superalloy at 800 and 1000 °C: Microstructure and oxide layer characterization. *Mater Charact* 161:110160. <https://doi.org/10.1016/j.matchar.2020.110160>
 50. Kayalı Y, Kanca E, Günen A (2022) Effect of boronizing on microstructure, high-temperature wear and corrosion behavior of additive manufactured Inconel 718. *Mater Charact* 191:112155
 51. Çarboga C (2021) Effect of V addition on tribocorrosion wear behavior of boride layer produced on AISI 1040. *Emerg Mater Res* 11(1):33–40
 52. Erdogan A, Kursuncu B, Günen A, Kalkandelen M, Gok MS (2020) A new approach to sintering and boriding of steels “Borosintering”: Formation, microstructure and wear behaviors. *Surf Coat Technol* 386:125482
 53. Turgut S, Günen A (2020) Mechanical properties and corrosion resistance of borosintered distalloy steels. *J Mater Eng Perform* 29(11):6997–7010
 54. Zhao X-Y, Togaru M, Guo Q-Y, Weinberger CR, Lamberson L, Thompson GB (2019) Carbon influence on fracture toughness of niobium carbides. *J Eur Ceram Soc* 39:5167–5173. <https://doi.org/10.1016/j.jeurceramsoc.2019.08.022>
 55. Tripathy M, Munther M, Davami K, Beheshti A (2020) Surface property study of additively manufactured Inconel 625 at room temperature and 510 °C. *Manuf Lett* 26:69–73. <https://doi.org/10.1016/j.mfglet.2020.10.001>
 56. Jeyaprakash N, Yang CH, Ramkumar KR (2020) Microstructure and wear resistance of laser clad Inconel 625 and Colmonoy 6 depositions on Inconel 625 substrate. *Appl Phys A* 126:455. <https://doi.org/10.1007/s00339-020-03637-9>
 57. Bai H-Q, Zhong L, Kang L, Liu J-B, Zhuang W-J, Lv Z-L, Xu Y-H (2021) A review on wear-resistant coating with high hardness and high toughness on the surface of titanium alloy. *J Alloys Compd* 882:160645. <https://doi.org/10.1016/j.jallcom.2021.160645>
 58. Hu Y, Watson M, Maiorino M, Zhou L, Wang WJ, Ding HH, Lewis R, Meli E, Rindi A, Liu QY, Guo J (2021) Experimental study on wear properties of wheel and rail materials with different hardness values. *Wear* 477:203831. <https://doi.org/10.1016/j.wear.2021.203831>
 59. Feng K, Chen Y, Deng P-S, Li Y-Y, Zhao H-X, Lu F-G, Li R-F, Huang Z-G, Li Z-G (2017) Improved high-temperature hardness and wear resistance of Inconel 625 coatings fabricated by laser cladding. *J Mater Process Technol* 243:82–91. <https://doi.org/10.1016/j.jmatprotec.2016.12.001>

60. González R, García MA, Peñuelas I, Cadenas M, Fernández MDR, Hernandez Battez A, Felgueroso D (2007) Microstructural study of NiCrBSi coatings obtained by different processes. *Wear* 263:619–624. <https://doi.org/10.1016/j.wear.2007.01.094>
61. Birol Y (2010) High temperature sliding wear behaviour of Inconel 617 and Stellite 6 alloys. *Wear* 269:664–671. <https://doi.org/10.1016/j.wear.2010.07.005>
62. Thomas C, Tait P (1994) The performance of Alloy 625 in long-term intermediate temperature applications. *Int J Press Vessel Pip* 59(1–3):41–49. [https://doi.org/10.1016/0308-0161\(94\)90140-6](https://doi.org/10.1016/0308-0161(94)90140-6)
63. Radu I, Li DY (2005) Investigation of the role of oxide scale on Stellite 21 modified with yttrium in resisting wear at elevated temperatures. *Wear* 259:453–458. <https://doi.org/10.1016/j.wear.2005.01.022>
64. Iwabuchi A (1985) Fretting wear of inconel 625 at high temperature and in high vacuum. *Wear* 106(1–3):163–175. [https://doi.org/10.1016/0043-1648\(85\)90108-5](https://doi.org/10.1016/0043-1648(85)90108-5)
65. Stott FH (1998) The role of oxidation in the wear of alloys. *Tribol Int* 31(1–3):61–71. [https://doi.org/10.1016/S0301-679X\(98\)00008-5](https://doi.org/10.1016/S0301-679X(98)00008-5)
66. Rahman MS, Ding J, Beheshti A, Zhang X, Polycarpou AA (2019) Tribology of incoloy 800HT for nuclear reactors under helium environment at elevated temperatures. *Wear* 436–437:203022. <https://doi.org/10.1016/j.wear.2019.203022>
67. Stott FH (2002) High-temperature sliding wear of metals. *Tribol Int* 35:489–495. [https://doi.org/10.1016/S0301-679X\(02\)00041-5](https://doi.org/10.1016/S0301-679X(02)00041-5)
68. Blau PJ (2010) Elevated-temperature tribology of metallic materials. *Tribol Int* 43:1203–1208. <https://doi.org/10.1016/j.triboint.2010.01.003>
69. Rahman MS, Ding J, Beheshti A, Zhang X, Polycarpou AA (2019) Helium tribology of Inconel 617 at elevated temperatures up to 950° C: Parametric study. *Nucl Sci Eng* 193(9):998–1012. <https://doi.org/10.1080/00295639.2019.1582315>
70. Kucuk Y, Doleker KM, Gok MS, Dal S, Altınay Y, Erdogan A (2022) Microstructure, hardness and high temperature wear characteristics of boronized Monel 400. *Surf Coat Technol* 436:128277. <https://doi.org/10.1016/j.surfcoat.2022.128277>

Publisher's Note Springer Nature remains neutral with regard to jurisdictional claims in published maps and institutional affiliations.

Springer Nature or its licensor (e.g. a society or other partner) holds exclusive rights to this article under a publishing agreement with the author(s) or other rightsholder(s); author self-archiving of the accepted manuscript version of this article is solely governed by the terms of such publishing agreement and applicable law.